NANO LETTERS
Cite This: Nano Lett. 2018, 18, 595−601
Letter
pubs.acs.org/NanoLett

Unusual Ferroelectricity in Two-Dimensional Perovskite Oxide Thin Films

Jinlian Lu,[†,‡] Wei Luo,[†,‡] Junsheng Feng,[†,‡] and Hongjun Xiang*[,†,‡]

[†]Key Laboratory of Computational Physical Sciences (Ministry of Education), State Key Laboratory of Surface Physics, and Department of Physics, Fudan University, Shanghai 200433, P. R. China

[‡]Collaborative Innovation Center of Advanced Microstructures, Nanjing 210093, P. R. China

Supporting Information

ABSTRACT: Two-dimensional (2D) ferroelectricity have attracted much attention due to their applications in novel miniaturized devices such as nonvolatile memories, field effect transistors, and sensors. Since most of the commercial ferroelectric (FE) devices are based on ABO_3 perovskite oxides, it is important to investigate the properties of 2D ferroelectricity in perovskite oxide thin films. Here, based on density functional theory (DFT) calculations, we find that there exist three kinds of in-plane FE states that originate from different microscopic mechanisms: (i) a proper FE state with the polarization along [110] due to the second-order Jahn−Teller effect related to the B ion with empty d-orbitals; (ii) a robust FE state with the polarization along [100] induced by the surface effect; (iii) a hybrid improper FE state with the polarization along [110] that is induced by the trilinear coupling between two rotational modes and the A-site displacement. Interestingly, the ferroelectricity in the latter two cases becomes stronger along with decreasing the thin film thickness, in contrast to the usual behavior. Moreover, the latter two FE states are compatible with magnetism since their stability does not depend on the occupation of the d-orbitals of the B-ion. These two novel 2D FE mechanisms provide new avenues to design 2D multiferroics, as we demonstrated in SrVO and CaFeO thin film cases. Our work not only reveals new physical mechanisms of 2D ferroelectricity in perovskite oxide thin films but also provides a new route to design the high-performance 2D FE and multiferroics.

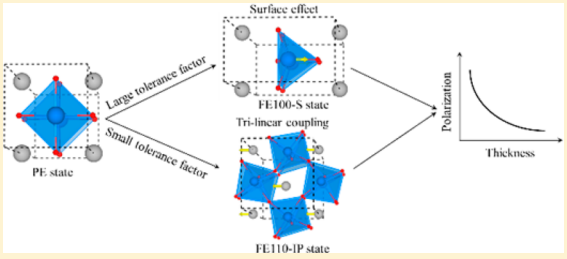

KEYWORDS: *Perovskite oxide thin film, ferroelectricity, two-dimensional multiferroics, first-principle calculations*

Ferroelectric (FE) materials can be widely used in many applications, such as sensors, actuators, and memories.[1−3] As demands for the size miniaturization of devices rises, the investigation of two-dimensional (2D) ferroelectrics becomes urgent and important. Very recently, Chang et al. discovered the robust in-plane ferroelectricity in atomic-thick SnTe and suggested to use it in a nonvolatile ferroelectric random access memory device.[4] Some other 2D in-plane FE materials were also proposed theoretically, such as hexagon honeycomb structures and their functionalized materials,[5−7] group IV−VI AB monolayer in the phosphorene-like structures,[8−11] and other III_2−VI_3 materials.[12] Since the commercial FE devices are mostly based on perovskite oxides, it is important to investigate the properties of 2D ferroelectricity in perovskite oxide thin films so as to make 2D FE devices based on the current technology.

Among the previous studies on perovskite oxide thin films, most of the attentions have focused on the critical thickness for the out-of-plane spontaneous polarization,[2,13−16] while there are only a few investigations on the in-plane ferroelectricity in perovskite oxides thin films. For example, Vanderbilt and co-workers studied in-plane ferroelectricity in $BaTiO_3$ surfaces with density functional theory (DFT) to find that the FE displacement of the surface Ti ion is larger (smaller) than that of the inner Ti ion in a TiO_2-terminated (BaO-terminated) slab.[17,18] Their results were reproduced by Tinte and Stachiotti[19] who employed an atomistic shell model to find that the in-plane ferroelectricity is more stable than the out-of-plane ferroelectricity for perovskite oxides thin films with the thickness up to 28 Å. Using the effective Hamiltonian method, Almahmoud et al. found that the Curie temperature of the in-plane ferroelectricity in $Pb(Zr_{0.5}Ti_{0.5})O_3$ thin films decreases as the thickness decreases.[20] Despite the progress made on the ferroelectricity in perovskite oxides thin films, several key issues remain to be addressed: (1) How will the FE properties change in ultrathin films compared to bulk? (2) Are there new FE mechanisms in perovskite oxides thin films? Hence, a comprehensive study on the ferroelectricity in perovskite oxides thin films is highly desirable.

In this work, we systematically investigate the in-plane ferroelectricity in the ABO_3 perovskite oxide ultrathin films with the thickness ranging from 1 to 5 unit cell (UC, in this work "*n*-UC" means that the system includes *n* BO_2 layers). Besides the usual FE state that is also present in bulk perovskite

Received: November 13, 2017
Revised: December 12, 2017
Published: December 12, 2017

DOI: 10.1021/acs.nanolett.7b04797
Nano Lett. 2018, 18, 595−601

oxide (e.g., bulk $BaTiO_3$), our DFT results show that there exist two novel kinds of FE states in perovskite oxides thin films, namely, a surface-effect induced robust FE state with polarization along the [100] direction, and a hybrid improper FE state with polarization along the [110] direction. Surprisingly, the FE polarization in these two FE states increases with decreasing the film thickness. We further demonstrate that these two kinds of FE states can be employed to design/predict new 2D magnetic multiferroics since they are compatible with partially filled d-orbitals of B.

Methods. The structural relaxation and electronic structure calculations are carried out by the Vienna ab initio simulation (VASP)[21] with the projector-augmented-wave (PAW) method.[22] The exchange-correlation energy is described by the Perdew–Burke–Ernzerh functional of the generalized gradient approximation (GGA-PBE function).[23] The cutoff energy is set to be 500 eV. A vacuum space more than 15 Å is used to avoid the interaction between neighboring slabs. To confirm the ground state of 2-UC BaTiO thin film with TiO_2 termination, we adopt a global optimization method based on the genetic algorithm.[26] The population size and number of generations are set to be 12 and 23, respectively. For magnetic systems, we adopt the DFT+U method[27] to deal with the strong electron correlation. The on-site repulsion U are set to be 3 and 4 eV for V and Fe ions, respectively. The exchange parameters J are set to be 1 eV for all magnetic ions.

To calculate the polarization (P) of FE slabs, we use the Berry phase method.[24,25] The polarization of the FE slab is computed with the PE slab as the reference. The PE slab was obtained by cutting the cubic bulk structure and a subsequent structural optimization.

Results and Discussion. For ABO_3 perovskite oxides, we can classify them into two categories according to the Goldschmidt tolerance factor,[28] which is an indicator for the stability and distortion of crystal structures. The Goldschmidt tolerance factor is defined as

$$t = \frac{r_A + r_O}{\sqrt{2}(r_B + r_O)}$$

where r_A and r_B are radii of the A-cation and B-cation, respectively, and r_O is the radii of the oxygen anion. If the perovskite oxide (e.g., $BaTiO_3$) has a relative large tolerance factor (i.e., $t \approx 1$), there is no tilting of the oxygen octahedra. However, if the tolerance factor of a perovskite oxide (e.g., $CaSnO_3$) is smaller than 1, significant tilting of the oxygen octahedra will take place. In this work, we will systematically study the FE properties for various perovskite oxides with different tolerance factors [see Table S1 in Supporting Information (SI)] to uncover new FE mechanisms in thin films. For the orientation of the thin films, we focus on the common [001] thin films. To make the surfaces nonpolar, we only study $A^{2+}B^{4+}O_3$ thin films so that both AO_2 and BO layers are neutral. We consider symmetric thin films with either AO_2 or BO terminations.

Two-Dimensional FE in Perovskite Oxides with a Large Tolerance Factor. For the perovskite oxides with a large Goldschmidt tolerance factor, we can further divide them into two categories according to whether they have empty 3d-orbitals at the B-site. In the following, we will investigate the ferroelectric properties in these two categories.

Perovskite Oxides with Empty 3d-Orbitals at the B-Site. Bulk $BaTiO_3$ is a widely studied FE material with a large polarization along the [111] direction in the lowest energy rhombohedral phase. Here, we first consider the case of TiO_2-terminated $BaTiO_3$ thin films. Note that the thin films do not have the same stoichiometry as bulk $BaTiO_3$ since both the top and bottom surfaces are terminated by the TiO_2 surfaces. We consider thin films up to the five unit-cells with the stoichiometry $Ba_{n-1}Ti_nO_{3n-1}$ (n = 2–5). The paraelectric phases of the $Ba_{n-1}Ti_nO_{3n-1}$ thin films are obtained by relaxing the slab cut from the cubic $BaTiO_3$ structure. To search for the stable structures of $Ba_{n-1}Ti_nO_{3n-1}$ thin films, we compute the phonon spectrum[29,30] of the paraelectric phase (see Figure 1a for the 2-UC case). We then follow the phonon displacements of the imaginary normal modes to obtain the stable structures (see part 1 of SI). With this method, we find that there exist two kinds of FE states for the BaTiO thin films (the antiferroelectric structures are found to have high energies, see Figure S2 of SI). One is the proper FE state along the [110] direction (named as FE 110-P); another is a special FE state along the [100] direction, which is later found to be induced by the surface effect (named as FE 100-S). The geometrical structures of 2-UC and 3-UC BaTiO thin films are shown in Figure 1 and Figure S3 of SI, respectively. In addition, we list the lattice constants of 2- to 5-UC BaTiO thin films in Table S2 of SI.

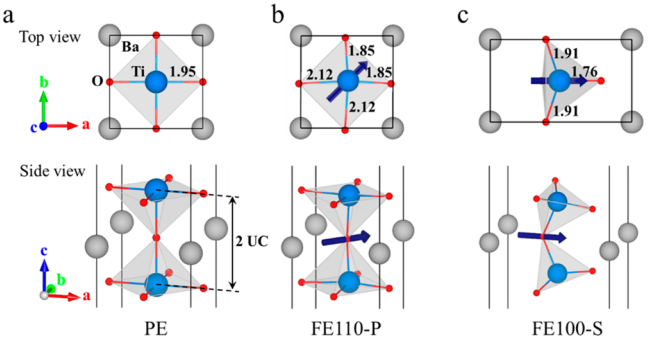

Figure 1. Top and side views of the geometrical structure of the 2-UC BaTiO thin film with TiO_2 termination for the (a) PE, (b) FE 110-P, and (c) FE 100-S phase. The blue arrow represents the polarization direction. Compared with the PE phase, the FE 100-S phase has a big distortion along the [100] direction. The numbers denote the Ti–O bond lengths (in Å).

For the FE 110-P state (Figure 1b), we find that it can also be obtained in another way: we first construct a slab by cutting the rhombohedral bulk $BaTiO_3$ with the FE polarization along [111], then we relax the slab to find that the out-of-plane polarization disappears due to the presence of the depolarization field, resulting in the FE 110-P state. Similar to the FE mechanism in bulk $BaTiO_3$, the ferroelectricity of the FE 110-P state of the thin film is also driven by the hybridization between the low-lying empty 3d states of the Ti-ion and the O 2p states, i.e., the second order Jahn–Teller effect.[31] We calculate the energy difference ($\Delta E = [E(\mathrm{PE}) - E(\mathrm{FE})]/n$, where n is the number of BO_2 layers) between the PE and FE 110-P states as a function of the thickness (see Figure 2a). We can see that as the thickness decreases the energy difference (ΔE) decreases. In addition, the value of polarization also decreases as the thickness decreases (see Figure 2a). Hence, we conclude that the ferroelectricity of the FE 110-P state becomes weaker as the thickness decreases, as found in the previous effective Hamiltonian simulations.[20]

DOI: 10.1021/acs.nanolett.7b04797
Nano Lett. 2018, 18, 595–601

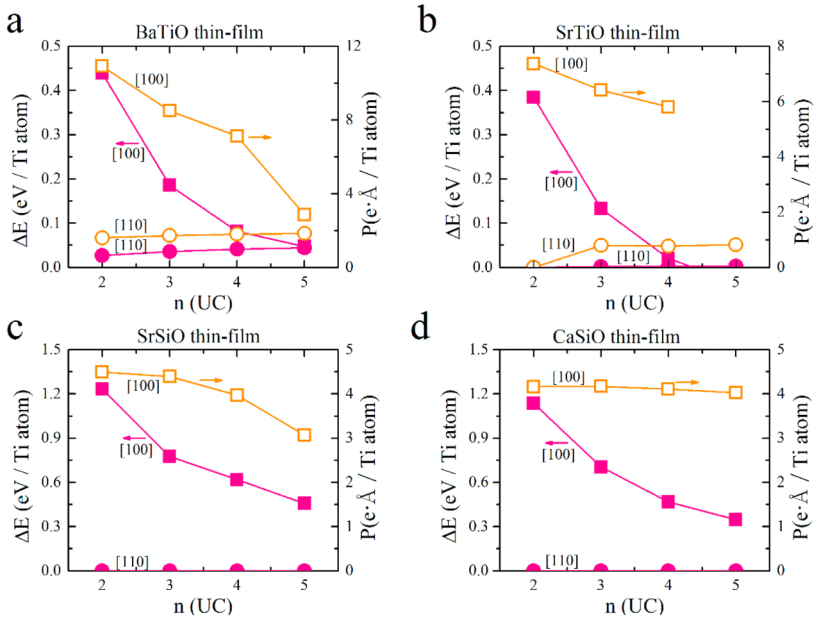

Figure 2. Energy difference (ΔE, remarked by red lines) between the PE state and FE (110-P and 100-S) state as a function of the slab thickness (n) for (a) BaTiO, (b) SrTiO, (c) SrSiO, and (d) CaSiO thin films with BO_2 termination. Here, ΔE is defined as $\Delta E = [E(\mathrm{PE}) - E(\mathrm{FE})]/n$, where E(FE) and E(PE) represent the total energies of FE and PE states, and n denotes the slab thickness (i.e., the number of BO_2 layers). The polarization (P) as a function of slab thickness for the FE 110-P and FE 100-S states are described by yellow lines. The ferroelectricity of the FE 110-P state becomes weaker as the thickness decreases, while the ferroelectricity of the FE 100-S state enhances as the thickness decreases.

For the FE 100-S state, we find that it has a big distortion compared with the PE structure (see Figure 1c for the crystal structure of 2-UC FE 100-S BaTiO thin film). In the 2-UC FE 100-S BaTiO thin film, there are two TiO_4 tetrahedra that share an oxygen corner. The two tetrahedra are rotated along the [010] axis in an antiphase manner. The lattice constant (a = 5.95 Å) along the a-axis (i.e., the direction of FE polarization) is much longer than the b-axis (b = 3.46 Å). We find that the FE 100-S state has a lower energy than the FE 110-P state. The stability of the FE 100-S state is also confirmed by a genetic algorithm simulation, which suggests that it is the lowest energy configuration for the 2-UC BaTiO thin film. The phonon spectrum[29,30] and ab initio molecular dynamic simulations indicate that the FE 100-S state is dynamical and thermally stable (see Figures S1b and S4 of SI). Strikingly, the energy difference ΔE between the PE state and FE 100-S state increases as the thickness decreases (see Figure 2a). In addition, the value of the polarization (see Figure 2a) increases as the thickness decreases. These facts indicate that the ferroelectricity becomes stronger as the thickness decreases, which is in sharp contrast with the usual trend. These FE 100-S BaTiO thin films are expected to be good 2D piezoelectric materials. Since the energy differences ΔE between the PE state and FE 100-S state for the 2-UC and 3-UC BaTiO thin films are very large (>0.15 eV/Ti), the FE polarization in 2-UC and 3-UC BaTiO thin films may not be switched by a currently available electric field. However, the 4-UC and 5-UC BaTiO thin films with the FE 100-S state have an appropriate energy barrier, suggesting that they are room temperature ferroelectrics that can be switched by an electric field.

Furthermore, we study the FE properties of BaTiO thin films with the BaO termination (see part 2 of SI for details). In this case, we find that the FE states are not stable for the 1-UC BaTiO thin film. When the thickness is larger than 2-UC, the FE 110-P state is more stable than the FE state with the polarization along [100], as shown in Figure S5b of SI. In addition, we find that the ferroelectricity (both the energy barrier and FE polarization) become weaker as the thickness decreases, similar to the case of the FE 110-P state of the TiO_2-terminated thin films.

It is noted that 4-UC BaTiO slabs were also studied previously by Vanderbilt and co-workers. It was suggested that the FE displacement of the surface Ti ions is larger than that of the inner Ti ion for the TiO_2-terminated slab, while the opposite was found for the BaO-terminated slab.[17,19,32] However, their studies are different from ours in several respects: (1) They only focused on the 4-UC slabs, while we study 1-UC to 5-UC thin films to see the dependence of ferroelectricity on the film thickness. (2) Since their initial intention is to simulate a surface instead of a free-standing thin film, they fixed the in-plane lattice constants of the slab to that of bulk FE $BaTiO_3$. In contrast, the in-plane lattice constants are fully relaxed in our current work. The different treatment of lattice constants leads to dramatically different results. Specifically, our study reveals a novel FE 100-S state with a large strain in the TiO_2-terminated thin films, and the ferroelectricity in the FE 100-S state enhances as the thickness decreases. The characteristic of this state will be totally different when the in-plane lattice constants of the slab are fixed to that of bulk $BaTiO_3$. In fact, the ferroelectricity of the FE state with the polarization along [100] becomes weaker as the thickness decreases if the in-plane lattice constants of the slab are fixed to that of bulk FE $BaTiO_3$ (see Figure S6 of SI).

Different from bulk $BaTiO_3$, bulk $SrTiO_3$ is a quantum paraelectric.[33] We also study the FE properties of TiO_2-terminated SrTiO thin films. We find that the FE 110-P state is hardly stable due to the weak ferroelectricity in bulk $SrTiO_3$. However, the FE 100-S state is very stable, and the ferroelectricity of the FE 100-S state enhances as the thickness decreases (see Figure 2b).

Perovskite Oxides without Empty 3d-Orbitals at the B-Site. Different from bulk $BaTiO_3$ and $SrTiO_3$, bulk $SrSiO_3$ has no

DOI: 10.1021/acs.nanolett.7b04797
Nano Lett. 2018, 18, 595−601

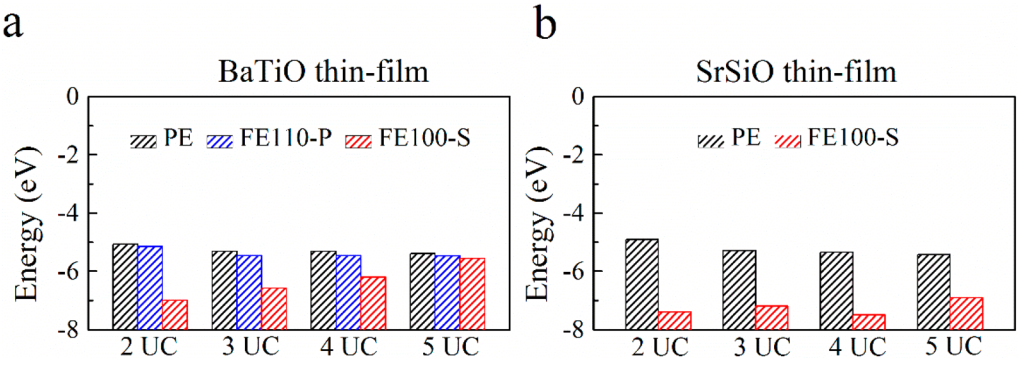

Figure 3. VBM of PE, FE 110-P, and FE 100-S states for the (a) BaTiO and (b) SrSiO thin films with BO_2 termination. The vacuum level is taken as the zero energy level. One can see clearly that the VBM of the FE 100-S state is lower than that of PE and FE 110-P states, especially for the 2-UC case.

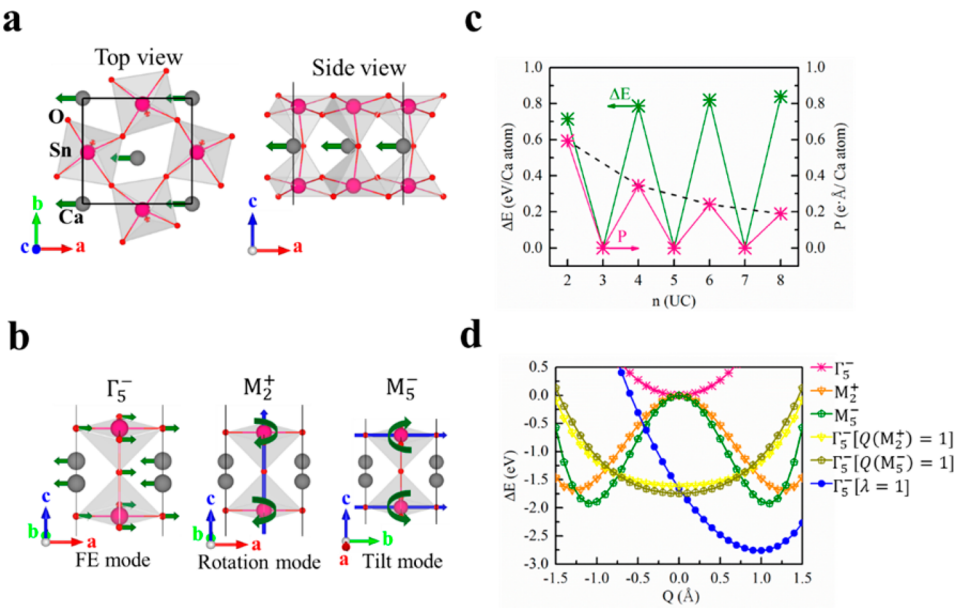

Figure 4. (a) Top and side view of the 2-UC SnO_2-terminated CaSnO thin films with the FE 110-IP state. The green arrows represent the direction of polarization. (b) Schematic illustration of the FE, rotation and tilt modes presented in the FE 110-IP state relative to the PE state. (c) Polarization as a function of thickness for the CaSnO thin films with both SnO_2 and CaO terminations. The polarization is zero in the case of odd thickness since the polarization is canceled by the adjacent CaO layers. (d) Total energies per unit cell as a function of the amplitude (Q) for the Γ_5^- (FE), M_2^+ (rotation), and M_5^- (tilt) modes. When only the FE Γ_5^- mode is present, the total energy minimum locates at $Q(\Gamma_5^-) = 0$. When either M_2^+ or M_5^- mode is condensed ($Q(M_2^+) = 1$ or $Q(M_5^-) = 1$), the total energy minimum also locates at $Q(\Gamma_5^-) = 0$. However, if both M_2^+ and M_5^- modes are present simultaneously (i.e., $Q(M_2^+) = 1$, $Q(M_5^-) = 1$), and $\lambda = Q(M_2^+) \times Q(M_5^-) = 1$), the total energy minimum locates near $Q(\Gamma_5^-) = 1$, suggesting that there is a hybrid improper ferroelectricity in 2-UC SnO_2-terminated CaSnO thin films.

empty 3d-orbitals at the B-site, thus is not a FE. It is expected that the FE 110-P state is not stable in SrSiO thin films. This is confirmed by the computed phonon spectrum of the 2-UC PE SrSiO thin film with SiO_2 termination, which shows no imaginary frequency (see Figure S7a of SI). Thus, we could not obtain any stable FE states by following the phonon eigenvectors of unstable phonons. Surprisingly, we find that the FE 100-S state of the SiO_2-terminated SrSiO thin films obtained by a substitution and subsequent relaxation of the FE 100-S structure of BaTiO thin films has a lower energy than the PE structure. This is striking since usually the PE state is not locally stable, and the FE state can be obtained from the soft mode theory. In the case of SrSiO thin films, the PE state itself is dynamically stable. It is the strain that greatly lowers the energy of the FE 100-S state of the SrSiO thin films with respect to the PE state (see part 3 of SI). In fact, the PE state of the 2-UC SrSiO thin film becomes unstable under a large strain (see Figure S8 of SI). We note that ferroelectricity of the FE 100-S state of SrSiO thin films is enhanced as the films get thinner (Figure 2c), similar to the cases of BaTiO and SrTiO thin films. To see the effect of the A-ion on the FE properties, we also investigate SiO_2-terminated CaSiO thin films to find that the results are similar (Figure 2d). The calculated phonon spectra show that the FE 100-S states in SrSiO thin films are dynamically stable (see Figure S7b of SI).

Origin of the FE 100-S Phase. As we described above, the FE 100-S state is robust since it can exist in perovskite oxides thin films regardless of whether the B-site contains empty 3d-orbitals or not. In order to understand its mechanism, we plot the valence band maximum (VBM) of the PE, FE 100-S, and FE 110-P for the 2- to 5-UC BaTiO and SrSiO thin films (see Figure 3). One can find that the VBM of the FE 100-S structure is much lower than that of PE and FE 110-P structures, especially for the 2-UC case. Since the VBM state is the highest

DOI: 10.1021/acs.nanolett.7b04797
Nano Lett. 2018, 18, 595−601

occupied energy level, the lowest VBM level of the FE 100-S structure is consistent with the fact that the FE 100-S structure has the lowest total energy. Our further analysis shows that the VBM states of both FE 110-P and FE 100-S structures are contributed by the surface O ions (see Figure S9 of SI). Considering also the fact that the ferroelectricity of the FE 100-S state becomes stronger as the thickness decreases (see Figure 2), we propose that the FE 100-S state originates from a surface effect. In fact, the bond lengths between Ti and the surface O atoms in the FE 100-S structure are much shorter than those in the PE and FE 110-P structures (see Figure 1). The shorter Ti−O bond means that the electrons of the surface O ions feel a stronger attractive potential of the Ti^{4+} ion in FE 100-S structure, leading to a lowering of the VBM level. In the case of SrSiO thin films, the stability of the FE 100-S state is due to a similar mechanism as that in the BaTiO thin films case. Besides, the fact that the Si atom tends to form the sp^3 hybridization with four neighboring O atoms further stabilizes the FE 100-S state (compare Figure 1a and c).

Two-Dimenisonal FE in Perovskite Oxides with a Small Tolerance Factor. Now, we turn to another kind of perovskite oxides with a small tolerance factor in which the tilting/rotation of oxygen octahedra takes place. In fact, the most common phase of bulk perovskite oxide adopts the so-called $GdFeO_3$-type structure.[34] This centrosymmetric phase (not FE) is orthorhombic with the *Pbnm* space group, and results from the condensation of an antiphase tilt about the [110] pseudocubic axis and an in-phase rotation about the [001] pseudocubic axis with respect to the ideal cubic perovskite structure. Here we take $CaSnO_3$ with a small tolerance factor as a typical example to investigate the FE properties of perovskite oxides thin films. Since bulk $CaSnO_3$[35] displays oxygen octahedron rotations, it is expected that oxygen octahedron rotations also take place in CaSnO thin films. Indeed, we find that the CaSnO thin films that are cut from the bulk *Pbnm* $CaSnO_3$ have lower energies than the PE CaSnO thin films that are cut from cubic perovskite structures (see Figure 4d). Interestingly, the SnO_2-terminated CaSnO thin films with even number of SnO_2 layers (e.g., 2-UC CaSnO thin film) are FE, while there is no FE polarization if the number of SnO_2 layers is odd (e.g., 3-UC CaSnO thin film, see Figure 4c). Since the FE polarization is along the [110] direction and the ferroelectricity is of the improper nature (as we will demonstrate later), we will name this FE state as the FE 110-IP state. The oscillation dependence of polarization on the number of SnO_2 layers can be explained as follows. In bulk *Pbnm* $CaSnO_3$, there is a Ca-site related antipolar mode, i.e., the Ca ions of two neighboring CaO_2 layers displace along the opposite directions.[36] This is also true in the case of CaSnO thin films. For example, in the 2-UC CaSnO thin film, the Ca layer displaces along the [110] direction, resulting in a net FE polarization since the polarization is not canceled (see Figure 4a). On the contrary, there is no net FE polarization in the 3-UC CaSnO thin film since the FE displacements from the two CaO layers cancel with each other. In this sense, the ferroelectricity in CaSnO thin films with three or more CaO_2 layers can be considered as ferroelectricity. Since only one CaO_2 layer contributes to the net polarization, the total polarization per unit volume decreases as the thickness increases (see Figure 4c). Thus, the ferroelectricity of the FE 110-IP state is enhanced when the film becomes thinner, similar to the case of the FE 100-S state.

We also examine the possibility of ferroelectricity in CaO-terminated CaSnO thin films. The main results are similar to the case of SnO_2-terminated CaSnO thin films: If the thin film contains an even number of CaO layers, there is no net polarization; otherwise, there is a net polarization (see Figure 4c).

In order to gain more insight into the microscopic mechanism of the FE 110-IP state, we examine the interaction between the different normal modes. By performing the mode decomposition,[37] we find that there are three distinct atomic distortions: a FE mode related to the Ca ion with the irreducible representation (irrep) Γ_5^-, an oxygen octahedron rotation mode with irrep M_2^+, and an oxygen octahedron tilt mode with irrep M_5^- in the SnO_2-terminated CaSnO thin film (see Figure 4b). The total energy is computed as a function of the amplitude of the individual Γ_5^-, M_2^+, and M_2^- modes relative to the parent structure. We obtain a double-well potential for the rotation and tilt distortions, whereas the FE mode is found to be stable, as shown in Figure 4d. When both rotation and tilt modes are present ($Q(M_2^+) = Q(M_5^-) = 1$), the FE mode lowers the total energy significantly. Our test calculations show that when only rotation or tilt mode is present ($Q(M_2^+) = 1$), or $Q(M_5^-) = 1$), the FE mode almost does not lower the total energy (see Figure 4d). These results suggest that there is a trilinear coupling between the FE, rotation, and tilt modes, i.e., $E \propto Q(\Gamma_5^-)Q(M_2^+)Q(M_5^-)$. This FE mechanism is similar to the hybrid improper ferroelectricity found in 3D bulk $Ca_3Ti_2O_7$ and [001] perovskite superlattices.[38−41] For this reason, we name the new 2D FE state as FE [110]-IP state.

Design Two-Dimensional Multiferroicity in Perovskite Oxide Thin Films. Two-dimensional multiferroics with coexisting ferroelectricity and magnetism[42−48] have attracted numerous interests due to their applications in novel nanoscale electric-write/magnetic-read memory devices. However, magnetism is often incompatible with ferroelectricity since the magnetism usually requires partially filled d-orbitals, while usual displacive ferroelectricity requires empty d-orbitals.[49] In this work, we discover two novel mechanisms (i.e., surface effect for the FE 100-S state and hybrid improper ferroelectricity for the FE 110-IP state) for 2D ferroelectricity, which does not rely on the presence of empty d-orbitals at the B-site. Hence, we expect that the FE and magnetic order can coexist in the perovskite oxides thin films with 3d magnetic ions at the B-sites. To demonstrate the possibility of designing 2D multiferroics with the new 2D FE mechanisms, we consider the 2-UC VO_2-terminated SrVO thin film and 2-UC CaO-terminated CaFeO thin film, whose lattice constants and polarization are listed in Table S4 of SI.

For 2-UC VO_2-terminated SrVO thin film, the lowest energy structure is found to be the FE 100-S state (see Figure 5). We consider four typical magnetic states of perovskite oxides (i.e., ferromagnetic state, A-type, C-type, and G-type antiferromagnetic state) and find that the magnetic ground state adopts a G-type antiferromagnetic state (see Table S3 of SI). The DOS calculations (see Figure S10 of SI) show it is a semiconductor with band gap about 1.20 eV. Therefore, 2-UC VO_2-terminated SrVO thin film is a 2D multiferroic with an antiferromagnetic magnetic order.

For 2-UC CaO-terminated CaFeO thin film, we find that the FE 110-IP structure has the lowest energy. For the magnetic order, we find that it has an A-type antiferromagnetic ground state along the *x* direction. Interestingly, this A-type order gives rise to a small canting magnetic moment of 0.006 μB/Fe along the *z* direction. The electronic structure analysis shows that it is

DOI: 10.1021/acs.nanolett.7b04797
Nano Lett. 2018, 18, 595−601

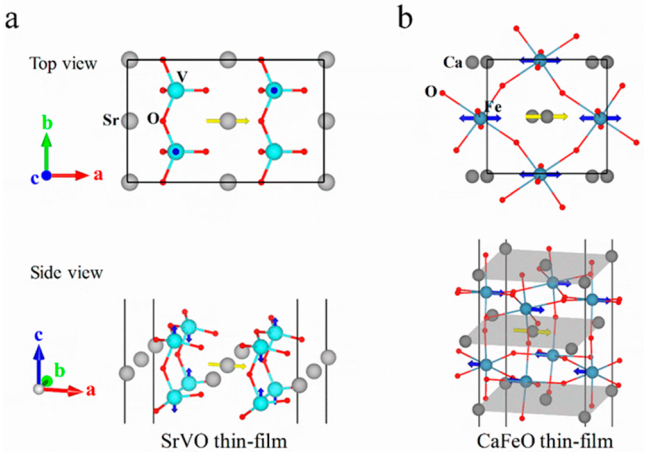

Figure 5. Top and side views of crystal structures of 2-UC (a) SrVO thin film with VO_2 termination and (b) CaFeO thin film with CaO termination. The blue and yellow arrows represent the direction of magnetic moments and total electric polarization, respectively.

a semiconductor with band gap about 0.92 eV. Therefore, 2-UC CaO-terminated CaFeO thin film is predicted to be a 2D multiferroic with a weak ferromagnetic moment. In addition, we check the effect of *U* and *J* values and find that our main results for the CaFeO and SrVO systems do not change for any reasonable *U* and *J* values (see Table S5 and S6 of SI).

Conclusion. In summary, we systematically investigate the ferroelectricity in 2D perovskite oxide thin films. We find there may exist three kinds of FE states, which stem from three different mechanisms: (i) a proper FE state with the polarization along [110] due to the second-order Jahn−Teller effect related to the B ion with empty d-orbitals; (ii) a robust FE state with the polarization along [100] induced by the surface effect; (iii) a hybrid improper FE state with the polarization along [110] that is induced by the trilinear coupling between two rotational modes and the A-site displacement. Interestingly, for the FE 100-S and FE 110-IP states, the ferroelectricity becomes stronger as the thickness decreases, which is distinct from the usual trend. Since the ferroelectricity in FE 100-S and FE 110-IP states does not rely on the empty d-orbitals, magnetism is compatible with these two FE states. In particular, we find the SrVO thin film is an antiferromagnetic semiconductor and CaFeO thin film is a multiferroic with a canted magnetic moment. Recently, the remote epitaxy through graphene was found to be an effective way to grow free-standing thin films. For example, homoepitaxial growth of GaAs(001) thin films on GaAs(001) substrates through monolayer graphene was achieved.[50] We expect that the free-standing perovskite oxide thin films studied in this work can be grown with a similar remote epitaxy approach.

■ ASSOCIATED CONTENT

Supporting Information

The Supporting Information is available free of charge on the ACS Publications website at DOI: 10.1021/acs.nanolett.7b04797.

Experimental details and supporting figures and tables (PDF)

■ AUTHOR INFORMATION

Corresponding Author

*E-mail: hxiang@fudan.edu.cn.

ORCID

Hongjun Xiang: 0000-0001-9465-5216

Author Contributions

J.L. and W.L contributed equally to this work.

Notes

The authors declare no competing financial interest.

■ ACKNOWLEDGMENTS

We thank K. Liu for valuable discussions. Work was supported by NSFC (11374056), the Special Funds for Major State Basic Research (2015CB921700), Program for Professor of Special Appointment (Eastern Scholar), Qing Nian Ba Jian Program, and Fok Ying Tung Education Foundation.

■ REFERENCES

(1) Scott, J. F. *Science* **2007**, *315* (5814), 954−959.
(2) Spaldin, N. A. *Science* **2004**, *304* (5677), 1606−1607.
(3) Lines, M. E.; Glass, A. M. *Principles and Applications of Ferroelectrics and Related Materials*; Oxford University Press: 1977.
(4) Chang, K.; Liu, J. W.; Lin, H. C.; Wang, N.; Zhao, K.; Zhang, A. M.; Jin, F.; Zhong, Y.; Hu, X. P.; Duan, W. H.; Zhang, Q. M.; Fu, L.; Xue, Q.-K.; Chen, X.; Ji, S.-H. *Science* **2016**, *353* (6296), 274−278.
(5) Di Sante, D.; Stroppa, A.; Barone, P.; Whangbo, M.-H.; Picozzi, S. *Phys. Rev. B: Condens. Matter Mater. Phys.* **2015**, *91* (16), 161401.
(6) Wu, M. H.; Dong, S.; Yao, K. L.; Liu, J. M.; Zeng, X. C. *Nano Lett.* **2016**, *16* (11), 7309−7315.
(7) Luo, W.; Xiang, H. *Angew. Chem., Int. Ed.* **2016**, *55* (30), 8575−8580.
(8) Fei, R. X.; Kang, W.; Yang, L. *Phys. Rev. Lett.* **2016**, *117* (9), 097601.
(9) Wu, M. H.; Zeng, X. C. *Nano Lett.* **2016**, *16* (5), 3236−3241.
(10) Wan, W. H.; Liu, C.; Xiao, W. D.; Yao, Y. G. *Appl. Phys. Lett.* **2017**, *111*, 132904.
(11) Mehboudi, M.; Fregoso, B. M.; Yang, Y. R.; Zhu, W. J.; van der Zande, A.; Ferrer, J.; Bellaiche, L.; Kumar, P.; Barraza-Lopez, S. *Phys. Rev. Lett.* **2016**, *117* (24), 246802.
(12) Ding, W. J.; Zhu, J. B.; Wang, Z.; Gao, Y. F.; Xiao, D.; Gu, Y.; Zhang, Z. Y.; Zhu, W. G. *Nat. Commun.* **2017**, *8*, 14956.
(13) Fong, D. D.; Stephenson, G. B.; Streiffer, S. K.; Eastman, J. A.; Auciello, O.; Fuoss, P. H.; Thompson, C. *Science* **2004**, *304* (5677), 1650−1653.
(14) Junquera, J.; Ghosez, P. *Nature* **2003**, *422* (6931), 506−509.
(15) Sai, N.; Kolpak, A. M.; Rappe, A. M. *Phys. Rev. B: Condens. Matter Mater. Phys.* **2005**, *72* (2), 020101.
(16) Gao, P.; Zhang, Z. Y.; Li, M. Q.; Ishikawa, R.; Feng, B.; Liu, H.-J.; Huang, Y.-L.; Shibata, N.; Ma, X. M.; Chen, S. L.; Zhang, J. M.; Liu, K. H.; Wang, E.-G.; Yu, D. D.; Liao, L.; Chu, Y.-H.; Ikuhara, Y. *Nat. Commun.* **2017**, *8*, 15549.
(17) Meyer, B.; Padilla, J.; Vanderbilt, D. *Faraday Discuss.* **1999**, *114*, 395−405.
(18) Padilla, J.; Vanderbilt, D. *Phys. Rev. B: Condens. Matter Mater. Phys.* **1997**, *56* (3), 1625.
(19) Tinte, S.; Stachiotti, M. G. *Phys. Rev. B: Condens. Matter Mater. Phys.* **2001**, *64* (23), 235403.
(20) Almahmoud, E.; Kornev, I.; Bellaiche, L. *Phys. Rev. B: Condens. Matter Mater. Phys.* **2010**, *81* (6), 064105.
(21) Kresse, G.; Furthmüller, J. *Phys. Rev. B: Condens. Matter Mater. Phys.* **1996**, *54* (16), 11169−11186.
(22) Kresse, G.; Joubert, D. *Phys. Rev. B: Condens. Matter Mater. Phys.* **1999**, *59* (3), 1758−1775.
(23) Perdew, J. P.; Burke, K.; Ernzerhof, M. *Phys. Rev. Lett.* **1996**, *77* (18), 3865−3868.
(24) Resta, R. *Rev. Mod. Phys.* **1994**, *66* (3), 899−915.

DOI: 10.1021/acs.nanolett.7b04797
Nano Lett. 2018, 18, 595−601

(25) King-Smith, R. D.; Vanderbilt, D. *Phys. Rev. B: Condens. Matter Mater. Phys.* **1993**, *47* (3), 1651−1654.
(26) Lu, X. Z.; Gong, X. G.; Xiang, H. J. *Comput. Mater. Sci.* **2014**, *91*, 310−314.
(27) Anisimov, V. I.; Aryasetiawan, F.; Lichtenstein, A. *J. Phys.: Condens. Matter* **1997**, *9* (4), 767−808.
(28) Liu, X. C.; Hong, R. Z.; Tian, C. S. *J. Mater. Sci.: Mater. Electron.* **2009**, *20* (4), 323−327.
(29) Parlinski, K.; Li, Z. Q.; Kawazoe, Y. *Phys. Rev. Lett.* **1997**, *78* (21), 4063−4066.
(30) Togo, A.; Oba, F.; Tanaka, I. *Phys. Rev. B: Condens. Matter Mater. Phys.* **2008**, *78* (13), 134106.
(31) Bersuker, I. B. *Chem. Rev.* **2013**, *113* (3), 1351−1390.
(32) Meyer, B.; Vanderbilt, D. *Phys. Rev. B: Condens. Matter Mater. Phys.* **2001**, *63* (20), 205426.
(33) Müller, K. A.; Burkard, H. *Phys. Rev. B: Condens. Matter Mater. Phys.* **1979**, *19* (7), 3593−3602.
(34) Geller, S. *J. Chem. Phys.* **1956**, *24* (6), 1236−1239.
(35) Vegas, A.; Vallet-Regi, M.; González-Calbet, J. M.; Alario-Franco, M. A. *Acta Crystallogr., Sect. B: Struct. Sci.* **1986**, *42* (2), 167−172.
(36) Bellaiche, L.; Íñiguez, J. *Phys. Rev. B: Condens. Matter Mater. Phys.* **2013**, *88* (1), 014104.
(37) Campbell, B. J.; Stokes, H. T.; Tanner, D. E.; Hatch, D. M. *J. Appl. Crystallogr.* **2006**, *39* (4), 607−614.
(38) Benedek, N. A.; Fennie, C. J. *Phys. Rev. Lett.* **2011**, *106* (10), 107204.
(39) Rondinelli, J. M.; Fennie, C. J. *Adv. Mater.* **2012**, *24* (15), 1961−1968.
(40) Bousquet, E.; Dawber, M.; Stucki, N.; Lichtensteiger, C.; Hermet, P.; Gariglio, S.; Triscone, J.-M.; Ghosez, P. *Nature* **2008**, *452* (7188), 732−U4.
(41) Zhao, H. J.; Íñiguez, J.; Ren, W.; Chen, X. M.; Bellaiche, L. *Phys. Rev. B: Condens. Matter Mater. Phys.* **2014**, *89* (17), 174101.
(42) Lee, M.; Hwang, J.; Choi, E. S.; Ma, J.; Dela Cruz, C. R.; Zhu, M.; Ke, X.; Dun, Z. L.; Zhou, H. D. *Phys. Rev. B: Condens. Matter Mater. Phys.* **2014**, *89* (10), 104420.
(43) Zhou, H. D.; Lumata, L. L.; Kuhns, P. L.; Reyes, A. P.; Choi, E. S.; Dalal, N. S.; Lu, J.; Jo, Y. J.; Balicas, L.; Brooks, J. S.; Wiebe, C. R. *Chem. Mater.* **2009**, *21* (1), 156−159.
(44) Hwang, J.; Choi, E. S.; Ye, F.; Dela Cruz, C. R.; Xin, Y.; Zhou, H. D.; Schlottmann, P. *Phys. Rev. Lett.* **2012**, *109* (25), 257205.
(45) Li, L.; Wu, M. *ACS Nano* **2017**, *11* (6), 6382−6388.
(46) Wu, M.; Burton, J. D.; Tsymbal, E. Y.; Zeng, X. C.; Jena, P. *Phys. Rev. B: Condens. Matter Mater. Phys.* **2013**, *87* (8), 081406.
(47) Tu, Z.; Wu, M.; Zeng, X. C. *J. Phys. Chem. Lett.* **2017**, *8* (9), 1973−1978.
(48) Yang, Q.; Xiong, W.; Zhu, L.; Gao, G.; Wu, M. *J. Am. Chem. Soc.* **2017**, *139* (33), 11506−11512.
(49) Hill, N. A. *J. Phys. Chem. B* **2000**, *104* (29), 6694−6709.
(50) Kim, Y.; Cruz, S. S.; Lee, K.; Alawode, B. O.; Choi, C.; Song, Y.; Johnson, J. M.; Heidelberger, C.; Kong, W.; Choi, S.; Qiao, K.; Almansouri, I.; Fitzgerald, E. A.; Kong, J.; Kolpak, A. M.; Hwang, J.; Kim, J. *Nature* **2017**, *544* (7650), 340−343.

DOI: 10.1021/acs.nanolett.7b04797
Nano Lett. 2018, 18, 595−601